

High-Efficiency Resonant Beam Charging and Communication

Yunfeng Bai, Qingwen Liu, *Senior Member, IEEE*, Xin Wang, *Senior Member, IEEE*,
Bin Zhou and Zhiyong Bu

Abstract—Simultaneous wireless information and power transfer (SWIPT) has been envisioned as an enabling technology for Internet of Things (IoT) by providing high-efficiency power transfer and high-rate data transmissions concurrently. In this paper, we propose a resonant beam (RB) charging and communication system utilizing the semiconductor gain medium and the telescope internal modulator (TIM). **The semiconductor gain medium has a better energy absorption capacity compared with the traditional solid-state one, the overall energy conversion efficiency can be enhanced, while TIM can concentrate the diverged beam into a small-size gain medium, thus the long-distance separation cavity for SWIPT can be achieved.** We establish an analytical model of this RB system for SWIPT and evaluate its beam transmission, output energy, and spectral efficiency. Numerical analysis shows that the proposed RB system can realize stable SWIPT over 10 meters, whose energy conversion efficiency is increased by 13 times compared with the original system using the solid-state gain medium without TIM, and the spectrum efficiency can be above 20 bit/s/Hz.

Index Terms—Simultaneous Wireless Information and Power Transfer; Resonant Beam; Semiconductor Gain Medium; Telescope Internal Modulator

I. INTRODUCTION

In the era of 5G and beyond, network capacity will continue to increase for rapidly growing number of devices [1]. At the same time, the energy consumption of mobile devices is also increasing dramatically to support high-performance communication and computation [2]. Facing these demands, various technologies have been promoted, e.g., millimeter-wave transmission, ultra-dense cloud radio access networks, and massive multiple-input multiple-output (M-MIMO) arrays, etc. [3], [4]. In terms of energy consumption, wireless power transfer (WPT) for providing unlimited energy supply is undoubtedly one of the most attractive solutions [3]–[5]. Compared with wired power supply, WPT is flexible and suitable for mobile devices; compared with battery, WPT is not restricted by battery’s capacity, weight, or volume [6], [7].

Simultaneous wireless information and power transfer (SWIPT) technology has attracted great attention from researchers to address the above issues. SWIPT technology is

Y. Bai, and Q. Liu, are with the College of Electronics and Information Engineering, Tongji University, Shanghai, China, (email: baiyf@tongji.edu.cn, qliu@tongji.edu.cn).

Xin Wang is with the Key Laboratory for Information Science of Electromagnetic Waves (MoE), Department of Communication Science and Engineering, Fudan University, Shanghai 200433, China (e-mail: xwang11@fudan.edu.cn).

B. Zhou, and Z. Bu, are with the Key Laboratory of Wireless Sensor Network and Communications, Shanghai Institute of Microsystem and Information Technology, Chinese Academy of Sciences, Shanghai, China, (email: bin.zhou@mail.sim.ac.cn, zhiyong.bu@mail.sim.ac.cn).

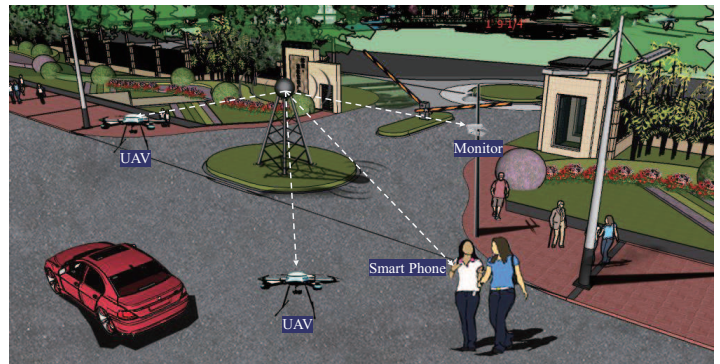


Fig. 1. Application scenarios of SWIPT

divided into two types: wide-beam broadcast and narrow-beam orientation. Wide-beam broadcast such as radio frequency (RF) can support wide-coverage [8]. However, it faces the difficulty of achieving high-power transmission due to energy dissipation and humans safety [9]. Narrow-beam orientation technology such as light beam-forming can support high-power transmission; however, the narrow beam leads to the challenge of positioning mobile receivers [10]. **To meet the requirements of both high-power and mobility, resonant beam system (RBS) was proposed [11]. The transmitter of the RBS is combined with the receiver to form a separate resonant cavity. The resonant beam generates in the cavity and carrying energy and information transfers between the transmitter and the receiver through the retro-reflectors.** Due to the energy concentration characteristics, RBS can achieve high power transfer [12]. By cooperating retro-reflectors, RBS enables self-alignment between the transmitter and the receiver for mobile SWIPT [13].

Since the light beam is the signal carrier in the RBS, the available bandwidth is larger than that of radio-frequency systems, which allows high-rate data transfer [14]. In addition, the light beam has no interference with radio frequency and thus the RBS is environmental-friendly [15]. What’s more, when the line of sight (LoS) between the transmitter and the receiver is blocked due to the intrusion of foreign objects, the cyclic reciprocating process of the resonant beam in the cavity will interrupt immediately. This prevents foreign objects from continuous radiative exposure, thus ensures safety [16].

Due to these remarkable advantages, the RBS has been applied in various SWIPT applications such as unmanned aerial vehicles (UAV), smartphones, laptops, etc. [17], [18].

The theoretical model, system design, deployment of the RBS have been studied in the literature. Zhang *et al.* in [11] first presented the principle and establish the analysis model of the RBS for energy transfer (a.k.a. distributed laser charging). In addition to the theoretical analysis, Zhang *et al.* verified that the energy transfer of the RBS using solid-state gain medium can achieve 2 W power transfer over 2.6 m in experiment [12]. To support multiuser access into the RBS, Xiong *et al.* proposed a time-division multiple access (TDMA) RBS design for wireless power transfer [19]. Xiong *et al.* also proposed the RBS communication design and the analytical model in [20]. Liu *et al.* presented the basic SWIPT model of the RBS and demonstrated its mobility using the retro-reflectors [13]. To evaluate the safety of the RBS, Fang *et al.* proposed an analytical model based on electromagnetic field analysis and assessed its safety with external object invasion [16].

The above studies explain the principle of RBS for SWIPT. Due to conversion and transmission loss, the existing RBS schemes can only achieve the transmission distance up to a few meters and the conversion efficiency of around 1% [12], which blocks its development. In this paper, we propose an RBS design using the semiconductor gain medium and the telescope internal modulator (TIM). Specifically, compared with the solid-state gain medium, the semiconductor has better energy absorption capability from the pump source. Thus, the energy level transition and population inversion efficiency are enhanced, threshold power decreases, and the overall conversion efficiency is improved. The TIM can concentrate the diverged beam into a small-size gain medium, thus the long-distance separation cavity for SWIPT can be achieved.

The contributions of this paper are summarized as follows:

- A resonant beam system design for SWIPT with enhanced conversion efficiency under long-range transmission by adopting the semiconductor gain medium and the telescope internal module (TIM) is proposed.
- An analytical model of the proposed system is presented, which describes the cavity stability, the beam propagation characteristics, the power output, and data transfer capability. A feasible evaluation method for system performance and a guidance for parameters optimization is provided.

The rest of the paper is organized as follows. In Section II, the model of the high-efficiency RBS involving the TIM and the semiconductor gain medium is described. In section III, the numerical evaluation of the system performance is depicted. The concerns on self-alignment and beam splitter is discussed in Section IV. In section V, the conclusion is presented.

II. SYSTEM MODELS

The system structure is shown in Fig. 2. The system is divided into three parts: transmitter, receiver, and free space cavity. The transmitter is mainly composed of a gain medium and a pump source. The pump source releases energy carrying the data signal in the form of optical radiation to the gain medium. Then, with the function of optical radiation, the gain medium occurs the stimulated absorption, spontaneous

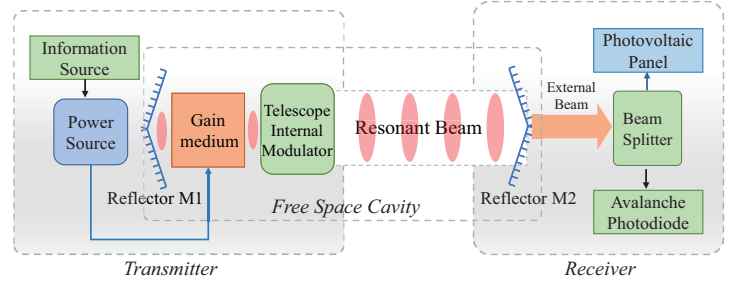


Fig. 2. High-efficiency resonant beam SWIPT system

emission, and stimulated emission, which builds the basis of resonant beam generation. The receiver mainly includes two parts: photovoltaic (PV) panel module and avalanche photodiode (APD) module [21], [22]. The PV module converts resonant beam energy into electrical power. The APD module is used to detect the data signal. The free space cavity is composed of a reflector M1, a TIM, and a reflector M2. Among them, M1 and M2 constitute the resonant cavity. Photons generated on the gain medium will oscillate back and forth within the cavity, which will finally form the resonant beam. The TIM is placed on the optical path in front of the gain, which is used to change the phase of the incident resonant beam for beam compression and promoting the beam incidence. Note that no matter one-to-many scenario or one-to-one scenario, the basal principle of transmission process is same. Thus, a one-to-one system model and performance analysis will only conduct in this paper.

A. Telescope Internal Modulator

The TIM structure consists of a concave lens and a convex lens that are placed in parallel and the center of the lens is collinear. The focal lengths of the concave lens 1 and the convex lens 2 are f_1 and f_2 . To make parallel incident resonant beams emerge in parallel, the focus of the convex lens in the direction of the concave lens coincides with the negative focus of the concave lens in the same direction to form an afocal optical system [23], that is, the relative distance of the two lenses satisfies:

$$l = f_1 + f_2. \quad (1)$$

After the incident cavity beam passes through the convex lens, the convex lens adjusts the beam phase converging the beam to the focal point. Then, through the reverse phase correction of the concave lens, the beam passes the concave lens and form a compressed beam. Finally, two tasks will be completed in the process: 1) beam compression; 2) beams emitted in parallel.

In order to define and analyze the transmission of resonant beams in space, we introduce the vector and matrix to accurately and strictly analyze. Based on the beam characteristics (straight line propagating), we can depict it as a vector $\vec{r} = (x, \theta_x)$, where x expresses the position parameter on the coordinate axis and θ_x represents the propagation direction of the beam. We assume that a beam at the origin of Z axis is transmitted in free space, from x_1 to x_2 , and its direction angle of transmission is θ_1 . Using the beam vector, it can

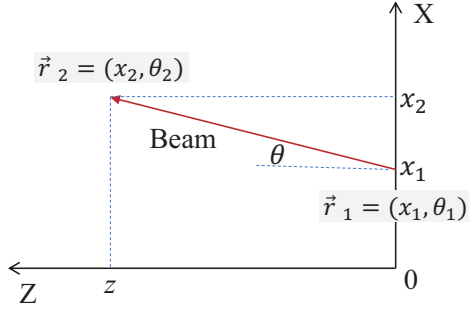


Fig. 3. Beam transmission express by vector

be expressed as $\vec{r}_1 = (x_1, \theta_1)$. Then, after the beam travels to z position along the Z axis, the beam vector becomes $\vec{r}_2 = (x_2, \theta_2)$. The process of \vec{r}_1 converts to \vec{r}_2 is presented in Fig. 3, which can be depicted as:

$$\vec{r}_2 = \begin{bmatrix} 1 & z \\ 0 & 1 \end{bmatrix} \begin{bmatrix} x_1 \\ \theta_1 \end{bmatrix} = \begin{bmatrix} x_2 \\ \theta_2 \end{bmatrix}, \quad (2)$$

where the direction angle meets $\theta = \theta_1 = \theta_2 \approx \tan \theta$, considering the value of the direction angle is small under the par-axial approximation. In summary, we can use the beam vectors and transmission matrices to describe the beam transfer, which is:

$$\begin{cases} \vec{r}^j = M\vec{r} \\ M = \begin{bmatrix} A & B \\ C & D \end{bmatrix}, \end{cases} \quad (3)$$

where \vec{r} and \vec{r}^j express the beam vectors before and after the converting, and M represents the transmission matrix. Further, when the beam passes through a series of optical components, the entire process can be expressed as the matrices of these components multiplied in the corresponding order.

The proposed TIM structure is shown in Fig. 4. When the beam enters, it will pass through lens 2 and free space with distance l , reaching lens 1, and finally pass through lens 1 with beam changing. We introduce the matrix M_T to describes these process, which is:

$$\begin{aligned} M_T &= \begin{bmatrix} 1 & 0 \\ -\frac{1}{f_2} & 1 \end{bmatrix} \begin{bmatrix} 1 & l \\ 0 & 1 \end{bmatrix} \begin{bmatrix} 1 & 0 \\ -\frac{1}{f_1} & 1 \end{bmatrix} \\ &= \begin{bmatrix} \frac{f_2-l}{f_1 f_2} & l \\ \frac{l-f_1-f_2}{f_1 f_2} & \frac{f_1-l}{f_1} \end{bmatrix}. \end{aligned} \quad (4)$$

Since $l = f_1 + f_2$ for the TIM, the equation (4) will become:

$$M_T = \begin{bmatrix} -\frac{f_1}{f_2} & l \\ 0 & -\frac{f_2}{f_1} \end{bmatrix}. \quad (5)$$

Under the action of M_T , any incident beam with vector \vec{r}_{in} (Fig. 4) will be transformed into \vec{r}_{out} with phase change. Correspondingly, the beam assembly takes on a compressed form.

Generally, the TIM can compress the incident beam, which increases the beam absorption ratio of the semiconductor gain medium under long-distance beam transfer. However, the

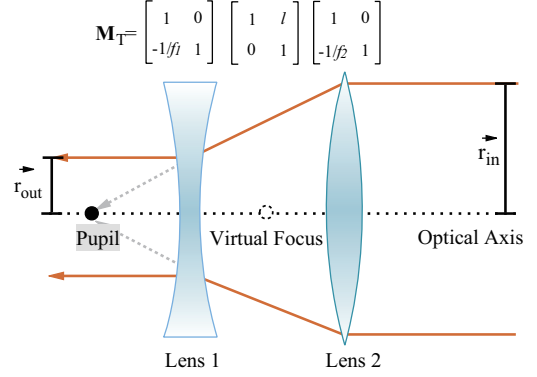


Fig. 4. Telescope internal modulator structure

introduction of the TIM will bring the challenge of the form-factor increase of the transmitter. Thus, reasonably designing the distance between TIM and M1, and elements position is necessary.

B. Stable Cavity and Beam Spot

In this paper, we proposed a high-efficiency RB scheme with semiconductor gain medium and TIM. To simplify the analysis process, we use typical curved mirrors instead of retro-reflectors as the reflectors on both sides of the cavity. To achieve reliable and durable SWIPT, the resonant cavity needs to keep stable. At this time, the cavity can restrict the resonant beam overflow and limit the beam to travel back and forth between the transmitter and receiver [24], [25].

To obtain the stability conditions of the cavity, we need to define the propagation process of resonant beam in the cavity at first. Taking M1 as the starting point, the beam propagating in the cavity will pass through lens 1, lens 2, and reflector M2 in sequence. Using matrices to express those process which is:

$$\begin{aligned} M_c &= M_{M2} M_{d2} M_{L2} M_1 M_{L1} M_{d1} M_{M1} \\ &= \begin{bmatrix} 1 & 0 \\ -\frac{1}{\rho_2} & 1 \end{bmatrix} \begin{bmatrix} 1 & d_2 \\ 0 & 1 \end{bmatrix} \begin{bmatrix} 1 & 0 \\ -\frac{1}{f_2} & 1 \end{bmatrix} \begin{bmatrix} 1 & l \\ 0 & 1 \end{bmatrix} \\ &\quad \begin{bmatrix} 1 & 0 \\ -\frac{1}{f_1} & 1 \end{bmatrix} \begin{bmatrix} 1 & d_1 \\ 0 & 1 \end{bmatrix} \begin{bmatrix} 1 & 0 \\ -\frac{1}{\rho_1} & 1 \end{bmatrix}, \end{aligned} \quad (6)$$

where M_{M1} , M_{M2} , M_{L1} , and M_{L2} express the matrix of reflector M1, M2 with curvature ρ_1 and ρ_2 , and lens L1, L2 with focal length f_1 and f_2 . M_{d1} , M_{d2} , and M_1 express the beam transfer in the free space with distances d_1 , d_2 and l . Note that we assume there are a plane mirror and a lens as a combination to replace the end mirror for matrix calculation. Through matrix calculation, we can get the specific expression

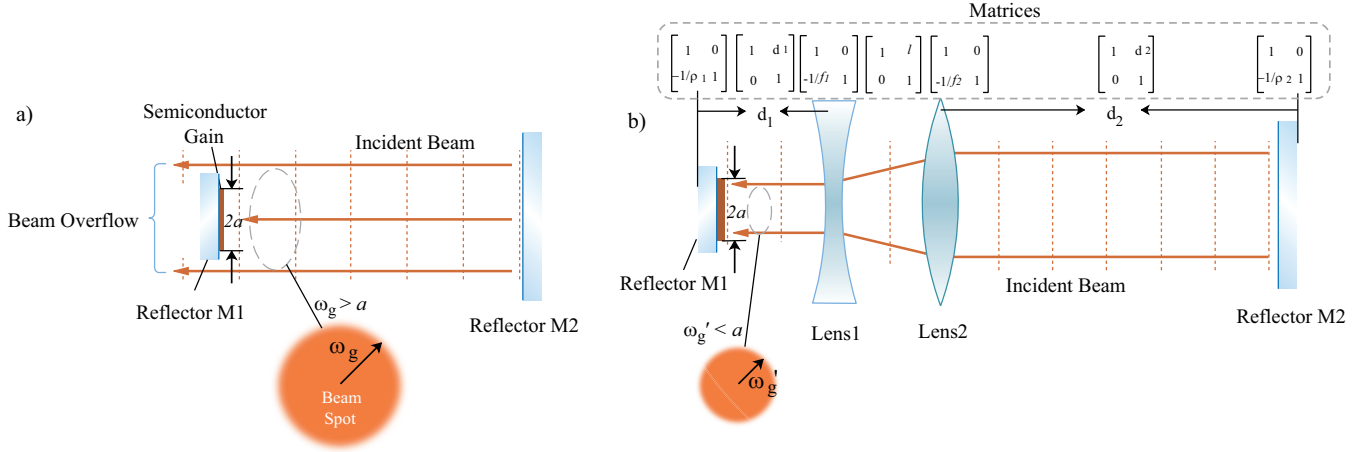


Fig. 5. Cavity structure of the RB system: a) resonant cavity without TIM, incident beam spot radius $\omega_g > a$ (gain radius); b) resonant cavity with TIM, incident beam spot radius $\omega'_g < a$

of matrix M_c :

$$M_c \begin{cases} A_c = M - \frac{L'' + L'M}{\rho_1} \\ B_c = \frac{L''}{M} + L'M \\ C_c = \left(\frac{L''}{M} - 1 + \frac{L'M}{\rho_2} \right) / \rho_1 - \frac{M}{\rho_2} \\ D_c = -\frac{L'' - 1}{M} - \frac{L'M}{\rho_2} \end{cases}, \quad (7)$$

where $L' = d_1 - f_1$, $L'' = d_2 - f_2$, and $M = -f_2/f_1$ which is introduced to evaluate the adjustment ability of TIM.

According to [24] and (7), the system can keep stable when the elements of M_c satisfy:

$$0 < \left(M - \frac{l + d_1 M + d_2/M}{\rho_1} \right) \cdot \left(\frac{1}{M} - \frac{l + d_1 M + d_2/M}{\rho_2} \right) < 1. \quad (8)$$

In the proposed, the reflector on the transmitter is a distributed Bragg reflector (DBR) integrated with the gain medium, which is a flat mirror ($\rho_1 = \infty$). At this time, the (8) can be simplified as:

$$0 < 1 - \frac{(f_1 - f_1 M) M + d_1 M^2 + d_2}{\rho_2} < 1. \quad (9)$$

From (9), we know that the stable cavity condition of the RB system changes with different parameters M , d_1 , d_2 , f_1 and ρ_2 .

Among them, M , d_1 , f_1 and ρ_2 are system structure parameters, and d_2 is the environmental variable which expresses the space distance between the transmitter and receiver. Therefore, through the stable cavity inequality, we can get: 1) the variation range of the system's transmission distance d_2 at different system structure parameters, and 2) the relationship between the structure parameters when the d_2 is determined.

Beam spot is the distribution of the beam in the vertical propagation direction, and its radius is usually used to evaluate

the lateral amplitude of the beam at a certain point. According to [24], [26], the beam spots radius on the reflectors of the resonant cavity can be defined by the transmission matrix elements. Since the gain medium is designed to be located on the M1 side, and the thickness of the gain is small. Therefore, it can be considered that the spot size on the gain is approximately equal to the spot size on M1. In this case, the beam spot radius on the gain medium can be given by:

$$\omega_g = \sqrt{\frac{\lambda}{\pi}} \sqrt{-\frac{B_c D_c}{A_c C_c}}, \quad (10)$$

where A_c , B_c , C_c , and D_c are the matrix elements of M_c mentioned above; λ is the wavelength of the resonant beam. The transmission loss is the main factor limiting the system transmission performance, which comes from the beam divergence, diffraction, and the mismatch between the beam and the elements' geometric boundary [27]. As shown in Fig. 5(a), when the beam is reflected from the receiver back to the transmitter, beam divergence generates after long-distance transmission causing the beam spot radius $\omega_g > a$ (geometric radius of gain medium). It makes part of the beam overflow and diffract on the edge of the gain medium, resulting in energy loss. Compared with the original system, the system cavity scheme in Fig. 5(b) introduces the TIM. The divergent resonant beam is modulated and compressed by the TIM before entering the gain medium ($\omega'_g < a$), which ensures entering effectively. As a result, transmission loss caused by diffraction will be suppressed and the long-distance separation cavity for SWIPT can be achieved.

C. Beam Generation on Semiconductor Gain

According to Fig. 2, the cavity includes reflectors M1, M2, TIM, and gain medium. Among them, TIM consists of two lenses with anti-reflective coating, whose absorption loss to the incident beam can be considered as 0. The resonant beam at any point propagates back and forth in the cavity and passes through these components, obtaining gain in the gain medium and outputting power on M2. During this process, after one

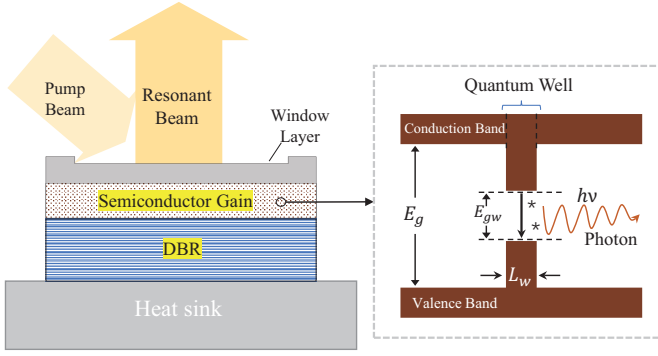


Fig. 6. Transmitter structure and operating principles of the semiconductor gain

round-trip, if the beam returns to the origin point and its energy is unchanged, we can conclude that the system achieves the balance of loss and gain. This equilibrium condition is called a threshold condition. Since the reflectivity of the reflectors M1 and M2 are R_1 and R_2 and the thickness of the gain medium is h , the threshold condition can be expressed as [28], [29]:

$$R_1 R_2 T_{\text{loss}} \exp(2gh) = 1, \quad (11)$$

where g represents the gain coefficient per unit length of the gain medium, T_{loss} expresses energy losses such as the absorption dispersion of reflectors and air, internal loss per unit thickness in the gain, etc. Each time the beam travels through the gain, the beam energy intensity will increase by $\exp(gh)$ times. R_1 and R_2 can be considered as the beam emission ratio of M1 and M2. Normally, the value of R_1 is set to 1, and the value of R_2 needs to be designed for optimal power output (APPENDIX A).

The proposed RB scheme applies the semiconductor medium as the gain for efficiency enhanced. Semiconductor gain utilizes the recombination of electrons in the conduction band and holes in the valence band to generate simulated radiation [30]. Compared with the solid gain medium, it has the following characteristics: 1) The active area and the cladding materials on both sides (window layer and DBR) have a band-gap difference forming a potential barrier. It will confine electrons and holes within the active area, which is conducive to the recombination of electrons and holes; 2) The active area and the cladding materials have a refractive index difference. When photons transfer on the material boundary, they will be reflected back to the active area. The light field is restricted to the active area, which causes more stimulated radiation; 3) The gain medium has a hetero-junction quantum well structure. This structure (Fig. 6) can further reduce the thickness of the active layer to the nano-level producing the quantum effect, which makes the limitation of carriers and light fields be further strengthened, and the forbidden bandwidth reduce from E_g to E_{gw} [31], [32]. Thanks to these characteristics, the loss of the particle conversion in semiconductor gain can be quite small, and the threshold value will be greatly reduced.

During the beam obtaining gain on the semiconductor medium, according to [33], the small signal material gain

coefficient g_0 , transparency carrier density N_0 , and the unit length gain coefficient g is used to express the threshold carrier density N_{th} :

$$N_{\text{th}} = N_0 \exp(g/g_0). \quad (12)$$

Among these parameters, N_0 and g_0 are material constant. Further, threshold P_{th} can be expressed by [33]:

$$P_{\text{th}} = N_{\text{th}} \frac{\epsilon h A_p}{\eta_{\text{abs}} \tau_{N_{\text{th}}}}, \quad (13)$$

where $h = N_w \cdot L_w$ represents the medium thickness (N_w : quantum well quantity; L_w : quantum well thickness), η_{abs} expresses the pump absorption efficiency, ϵ is photon energy, A_p is the effective pump area, and $\tau_{N_{\text{th}}}$ is carrier lifetime which can be depicted by [33]:

$$\tau_{N_{\text{th}}} = (\alpha + \beta N_{\text{th}} + \gamma N_{\text{th}}^2)^{-1}, \quad (14)$$

where α , β and γ express system recombination coefficients. Then, according to the cyclic power principle [29], the beam output power on the M2 can be depicted as:

$$P_{\text{beam}} = \frac{2(1 - R_2)}{(1 + R_2)[\delta_t - \ln R_2]} (P_P - P_{\text{th}}), \quad (15)$$

where $P_P = \eta_P P_{\text{in}}$ expresses the input pump energy, and $\delta_t = 1 - T_{\text{loss}} R_1$ is introduced to define the energy loss including the absorption, reflection, refraction of elements, the diffraction and the overflow loss of the beam. Furthermore, the conversion efficiency of the P_{in} to P_{beam} is:

$$\eta_b = \frac{2(1 - R_2)}{(1 + R_2)[\delta_t - \ln R_2]} \left(\eta_P - \frac{P_{\text{th}}}{P_{\text{in}}} \right), \quad (16)$$

where P_{in} is the input electric power and η_P is the conversion efficiency of the P_{in} to P_P that is a constant based on the pump source characteristic.

D. Energy Harvesting and Data Receiving

We have got the external beam with signal on the reflector M2 at the receiver. Then, we use a beam splitter to divide the external beam into two. One part will be transferred to the PV cell for power charging. The other part will be caught by the APD for data receiving.

1) *Energy harvesting*: This part of the external beam separated by the beam splitter is transmitted to the surface of the photovoltaic cell through a homogenizing waveguide. Then, the beam will be converted into electrical power output through photoelectric conversion. This process can be expressed by the following formula [34]:

$$\begin{cases} P_p = \mu P_{\text{beam}}, \\ P_{\text{E}_{\text{out}}} = a_1 P_p + b_1, \end{cases} \quad (17)$$

where μ is the power split ratio, P_p expresses the beam power received by the PV. The parameter a_1 is the slope efficiency of photoelectric conversion, and b_1 is the threshold power of PV. It is worth noting that, to simplify the simulation process, according to the experimental results of [11], $P_{\text{E}_{\text{out}}}$ is expressed by a linear model, where the PV is under ideal heat dissipation and receiving area conditions. In practice, the beam energy absorbed by PV is limited, it is expected that the

conventional linear EH model is only accurate for the specific scenario when the received powers at the receiver is in a constant power range and the nonlinear EH model has a better applicability [35]. Finally, the end to end energy conversion efficiency is depicted as:

$$\eta_{\text{Eout}} = \frac{a_1 P_p + b_1}{P_{\text{in}}}. \quad (18)$$

2) *Data receiving*: The remaining part of the external beam separated by the beam splitter will act on the APD. The APD converts the optical signal into an electrical signal while receiving the data. This process can be depicted as:

$$\begin{cases} P_D = (1 - \mu)P_{\text{beam}}, \\ P_{D_{\text{out}}} = \nu P_D, \end{cases} \quad (19)$$

where ν is the optical-to-electrical conversion responsivity of APD.

When APD is receiving data, photoelectric conversion will produce thermal noise and shot noise. Among them, thermal noise can be expressed by the following formula [36]:

$$n_{\text{thermal}}^2 = \frac{4kTB_x}{R_L}, \quad (20)$$

where k is the Boltzmann constant, T is the background temperature, and R_L is the load resistor. Moreover, the formula about the shot noise factor is [36]

$$n_{\text{shot}}^2 = 2q(P_{D_{\text{out}}} + I_{\text{bg}})B_x, \quad (21)$$

where q is the electron charge, B_x is the bandwidth, I_{bg} is the background current. At this point, the additive white Gaussian noise (AWGN) of the communication module can be defined:

$$N_M^2 = n_{\text{shot}}^2 + n_{\text{thermal}}^2. \quad (22)$$

Finally, we can obtain spectral efficiency of the system as [37]:

$$\tilde{C} = \frac{1}{2} \log_2 \left(1 + \frac{P_{D_{\text{out}}}^2}{2\pi e N_M^2} \right), \quad (23)$$

where e is the natural constant.

III. NUMERICAL EVALUATION

In this section, we will evaluate the proposed system performance by analyzing the transmission distance, beam radius on the gain, energy output, and channel capacity.

A. Stable Transmission Distance

From the principle in Section II.C, it is known that for the beam to continuously reciprocate oscillation between the receiver and the transmitter, the cavity needs to be stable. A highly stable resonant cavity can effectively constrain the transmission of the resonant beam, which is the prerequisite for long-distance transmission of the resonant beam. In the RB system, since the TIM is introduced in this system, the influence of the TIM structure on the transmission distance should be analyzed.

1) *Parameter Setting*: The system's resonant cavity is consisted of two curved mirrors as the beam reflector. The gain medium is composed of semiconductor material GaAsP,

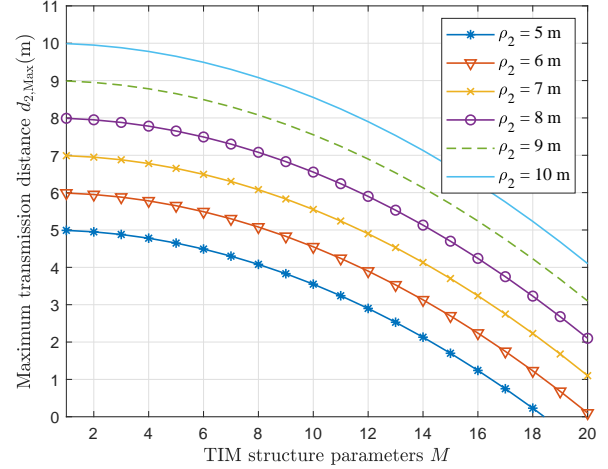


Fig. 7. Maximum transmission distance versus TIM structure parameter with different curvature values of the reflector M2

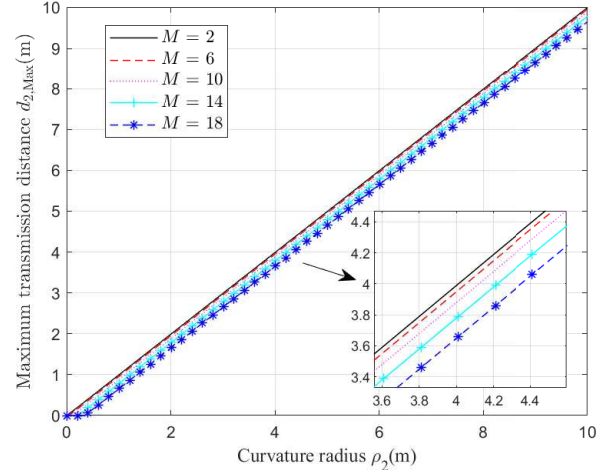


Fig. 8. Maximum transmission distance versus curvature of reflector M2 with different TIM structure parameter

which is set adjacent to the M1 and generates resonant beam with 980 nm wavelength. According to Section II.C, the reflector M1 made by DBR is a plane mirror with an infinite radius of curvature. To meet the stability cavity conditions and constrain the beam to maintain par-axial propagation, the M2 is set as a concave mirror whose radius of curvature is ρ_2 . Moreover, we use the maximum transmission distance $d_{2,\text{Max}}$ to represent the extreme value of d_2 when the stable cavity condition is satisfied ($d_{2,\text{Max}}$ is an ideal value which represents the system's transmission capability, in reality, the transmission distance of the system will be reduced by the energy attenuation such as air absorption). The TIM is positioned on the side of the gain medium, and its position parameter is set to $d_1 = 10$ mm relative to the gain chip. The focal length of the concave lens of the TIM is designed as $f_1 = -5$ mm.

2) *Calculation results and analysis*: Fig. 7 presents the relationship of the system's maximum transmission distance

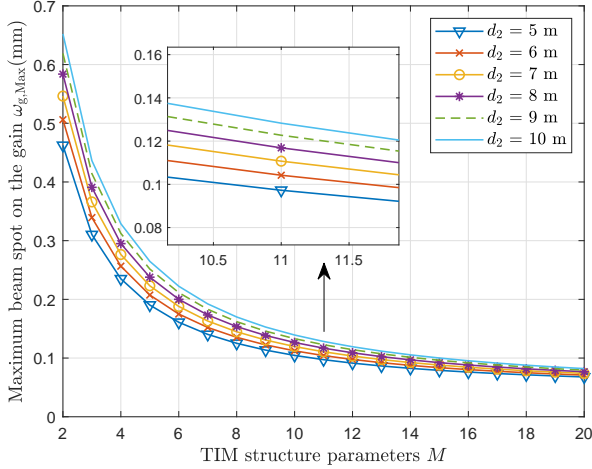


Fig. 9. Maximum beam radius on the gain versus TIM structure parameter for different curvature of reflector M2

and TIM structure parameters. As is shown, curves present a downward trend with an increasing M . When M reaches a certain large value, $d_{2,\text{Max}}$ will become 0 and the beam transmission is terminated. In addition, the transmission distance is affected by the curvature of the M2 mirror. When M is fixed, a large value of ρ_2 causes a longer effective transmission distance of the system. Furthermore, to present this influence brought by ρ_2 , we perform additional numerical analysis and these results are presented in Fig. 8. The plot shows that ρ_2 and $d_{2,\text{Max}}$ have a linear relationship. $d_{2,\text{Max}}$ increases as ρ_2 increases. Numerically, the value of $d_{2,\text{Max}}$ is almost equal to ρ_2 , and $d_{2,\text{Max}}$ is capable of reaching 10 meters.

In summary, excessive M will influence the stability of the cavity, resulting in distance decrease. Besides, the reflector M2 affects the amplitude of the incident resonant beam. A large value of the curvature of M2 causes a stronger adjustment and convergence ability to the resonant beam, which is beneficial to the stability of the cavity during long-distance transmission. Therefore, through increasing ρ_2 , the decrease in $d_{2,\text{Max}}$ can be compensated.

B. Resonant Beam Radius on Gain Medium

In order to suppress the transmission loss, the proposed RB system introduce a built-in TIM, which can modulate the phase of the beam to achieve the beam compression. To evaluate the compression performance, we focus on the beam spot on the gain medium, analyzing its radius changes with different structure parameters.

1) *Parameter Setting*: Since the intensity cross-section of the fundamental mode beam is circular, we use the spot radius to evaluate the change of the beam. Besides, considering the beam spot radius will be different at different distances, we take the maximum value of the spot radius $\omega_{g,\text{Max}}$ on the gain medium to analyze. We set end-end distances d_2 from 5 m to 10 m, and TIM structure parameter M as the inspection point, respectively. Then, we can analyze the relationship of the M and ρ_2 on $\omega_{g,\text{Max}}$.

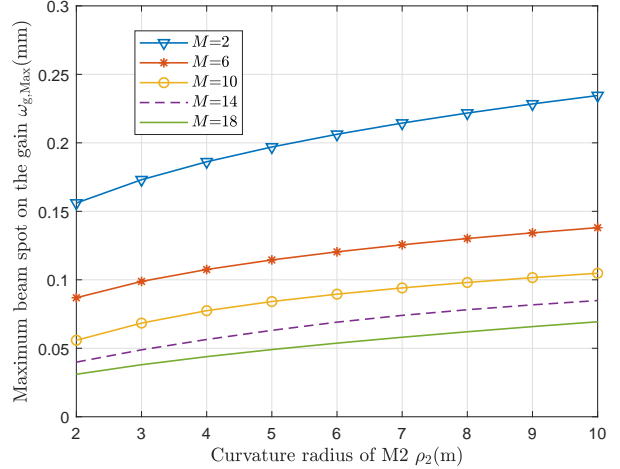


Fig. 10. Maximum beam radius on the gain versus curvature of reflector M2 with different TIM structure parameter

2) *Calculation results and analysis*: Fig. 9 depicts the relationship of the TIM structure parameter M and the maximum beam spot radius $\omega_{g,\text{Max}}$. When the value of M increases, the $\omega_{g,\text{Max}}$ shows a downward trend. When M is in the range of 2 to 6, the beam radius decreases rapidly, and when M is greater than 12, the decline of the beam spot tends to be gentle. What's more, the beam radius can be compressed from 0.65 mm to below 0.08 mm, which is only 1/8 of the initial beam radius. The result proves the beam compression ability of TIM; the compression capacity will increase with the increase of M . However, this compression capacity is limited. When the M is beyond the range, the compression tends to be stable. In addition, the curvature of the M2 will also affect the spot radius. Fig. 10 shows the situation of ρ_2 versus $\omega_{g,\text{Max}}$. As is shown from the curves, $\omega_{g,\text{Max}}$ presents an upward trend with the increase of ρ_2 . What's more, the curve tends to be flat as the value of M increases. Generally, the effect brought by ρ_2 is relatively small, specifically when the value of M is large.

According to the aforementioned analysis, preliminary conclusions can be obtained that the TIM can effectively compress the incident beam, which ensures that the resonant beam can enter the micron-level size semiconductor gain without causing large beam loss. Combining the conclusions in Part A, the system can achieve long-distance and high beam compression at the same time by matching the M and ρ_2 reasonably.

C. Energy Output

After the stable cavity condition of the system is established, with the energy accumulating, the external beam will eventually emerge from reflector M2. Then, it will enter the PV and APD respectively under the function of the beam splitter, realizing the electric power output and data reception. To evaluate the performance of the power output, we first calculate and analyze the power and energy conversion efficiency of the external beam before entering the beam splitter. Then, we set the splitting ratio μ of the beam splitter to 1, and analyze the total conversion efficiency of the system

TABLE I
PARAMETERS OF THE GAIN MEDIUM

Parameter	Symbol	Value
Gain factor	g_0	2000 cm^{-1}
Transparency carrier density	N_0	$1.7 \times 10^{18} \text{ cm}^{-3}$
Light quantum	ϵ	$2.46 \times 10^{-22} \text{ J}$
Longitudinal confinement factor	Γ	2.0
Path loss coefficient	T_{loss}	0.99
Quantum well thickness	L_w	8 nm
Quantum well quantity	N_w	14
Monomolecular recombination coefficient	α	10^7 sec^{-1}
Bimolecular recombination coefficient	β	$10^{-10} \text{ cm}^3/\text{sec}$
Auger recombination coefficient	γ	$10^{-30} \text{ cm}^6/\text{sec}$

when it is only used for energy harvesting for evaluating the efficiency improvement of the proposed system compared with the original RB charging system.

1) *Parameter Setting*: The gain medium is made of GaAsP. According to the material properties [33], we set the characteristic parameters such as light quantum, gain factor, etc. and listed them in Table I. The pump source adopts a commercial high-efficiency laser diode whose electro-optical conversion efficiency η_P is 0.7. The pump beam wavelength is 808 nm, and the diameter of the pump area is 100 μm . Besides, the beam energy receiver is PV cell. Its structure parameters a_1 and b_1 are set as 0.3487 and -1.535, respectively [11].

2) *Calculation results and analysis*: Fig. 11 describes the change of the external beam power and the output electrical power on the input power. As can be seen, both P_{beam} and P_{out} has a linear relationship with the input power. As the input power increases, the value of them will increase. What's more, the threshold power (intercept distance) is small. For instance, when the value of R_2 takes 0.93, the threshold of the system is only a few watts. Besides, through simulating separately by changing the parameters of R_2 , we discover that the slope efficiency changes with the R_2 changing (Analysis of the impact of R_2 on the P_{beam} is presented in Appendix A). When the reflectivity varies from 0.9 to 0.99, the slope efficiency presents an upward trend. Numerically, when R_2 takes 0.93, the value of P_{out} can be 13 W at $P_{\text{in}}=100 \text{ W}$.

Fig. 12 presents the curves of energy conversion efficiency versus input power. The conversion efficiency performance with different R_2 shows a similar tendency. Overall, with P_{in} increasing, η_b and η_E will rise rapidly first and then stabilize. When R_2 takes an appropriate value, such as 0.87, 0.9 and 0.93, the beam power conversion efficiency η_b can reach 40%. Besides, similar to the beam power curves, the reflectivity of the M2 also has an impact on the conversion efficiency. Preliminary conclusions can be drawn that a greater reflectivity will cause conversion efficiency to decrease. But, since the effect is disorderly, we have further explored the influence of reflectivity, and this analysis of R_2 on the η_b is available in Appendix A. Furthermore, from the curve of η_E ($\mu=1$), the end-end conversion efficiency of the system is nearly 13% at $P_{\text{in}}=100\text{W}$, while the efficiency of the original system is just about 1% and has a larger threshold power [12]. Overall, the end-end conversion efficiency of the proposed system is 13 times that of the traditional system.

According to the numerical results above, a brief summary

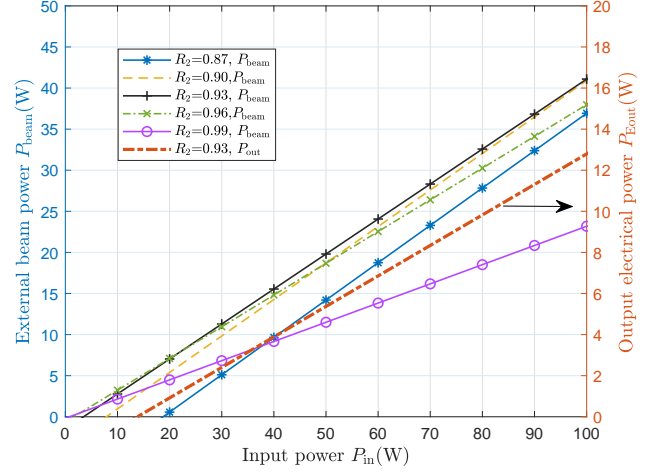


Fig. 11. External beam power and output electrical power versus input power for different reflectivity of reflector M2

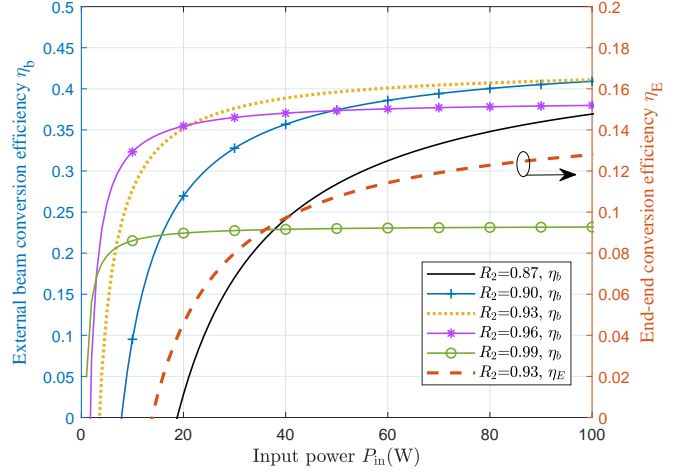


Fig. 12. End-end and external beam conversion efficiency as a function of input power for different M2's reflectivity

can be obtained that thanks to the TIM's spot compression and the high photon conversion of the semiconductor gain, the scheme we proposed in this paper, can effectively enhance the conversion efficiency of the system on the original basis.

D. Channel Capacity

After passing the beam splitter, part of the external beam will be caught by the APD for data receiving.

1) *Parameter Setting*: In the proposed system, the environment temperature is taken as $T=300 \text{ K}$, the electronic charge q is $1.6 \times 10^{-19} \text{ C}$, and the Boltzmann constant k is $1.38 \times 10^{-23} \text{ J/K}$. The APD for light signal receiving is commercial sensors for 980 nm wavelength. According to [36], [38]–[40], we set the conversion responsivity of the APD $\nu=0.6 \text{ A/W}$, the noise bandwidth $B_x=811.7 \text{ MHz}$, the background current $I_{\text{bg}}=5100 \mu\text{A}$, and the load resistance $R_L=10 \text{ K}\Omega$.

TABLE II
COMPARISON OF EXISTING SWIPT SCHEMES

Schemes&Authors	Input Power	Harvested Energy	Data Transfer	Conversion Efficiency	Transmission Distance
VL-based; Ma <i>et al.</i> [41]	316.2 W	2.96 mW	6 bit/s/Hz	$0.38 \times 10^{-4}\%$	1.5 m
VL-based; Abdelhady <i>et al.</i> [42]	450 W	0.38 mW	8 bit/s/Hz	$8.44 \times 10^{-5}\%$	3.0 m
RF-based; Krikidis <i>et al.</i> [43]	10 W	5 mW	7 bit/s/Hz	$5 \times 10^{-2}\%$	10 m
RF-based; Lu <i>et al.</i> [44]	4 W	$5.5 \mu\text{W}$	not stated	$1.375 \times 10^{-4}\%$	15 m
This work	100 W	13 W	20 bit/s/Hz	13%	10 m

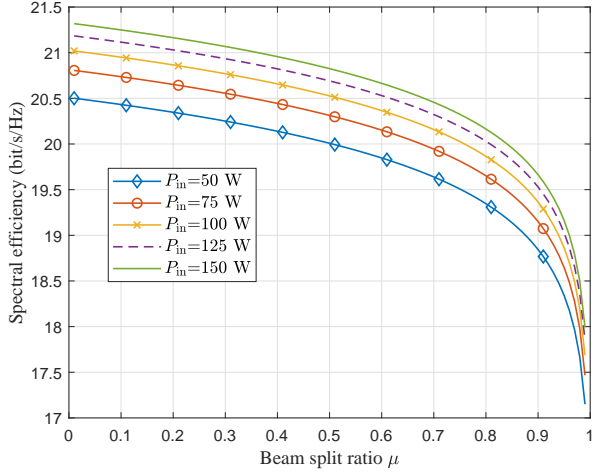


Fig. 13. Spectral efficiency versus beam split ratio with different input power

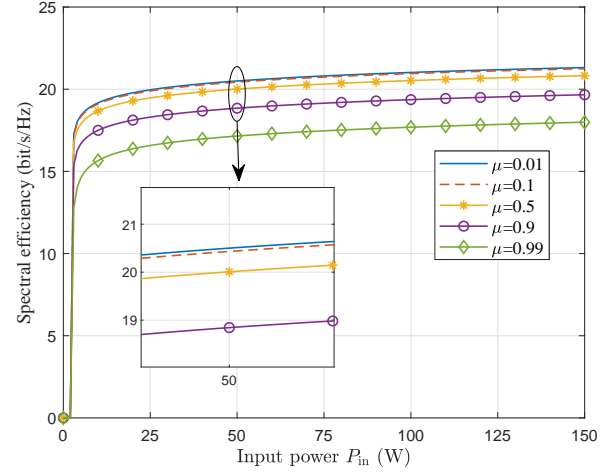


Fig. 14. Spectral efficiency versus input power for different beam split ratio

2) *Calculation results and analysis:* Fig 13 depicts curves of split ratio versus spectral efficiency. The curve shows a downward trend with an increase of μ . The decline of the curve is relatively gentle at the beginning. When μ is greater than 0.8, \tilde{C} begins to drop sharply. What's more, a large input power will make the curve move upward, which causes the overall value of \tilde{C} to become large. We further explore the change of the spectral efficiency from input power which is presented in Fig. 14. As can be seen, when the APD receives the beam power, the spectral efficiency will fast rises to a larger value. Then, with the input power continues to increase, the spectral efficiency of the system will be stable. From the theoretical principle presenting in Section II, $1-\mu$ represents the proportion of external beam entering the APD, which means the larger μ , the less beam energy is allocated to the APD.

Combining the above analysis, we can know that the spectral efficiency of the APD is affected by the amount of beam energy that enters. The greater the input beam energy, the higher spectral efficiency of the APD will obtain. However, this influence is relatively limited. Taking $\mu = 0.01$ (situation that most energy is split to APD) as an instance, when P_{in} increases from 50W to 150W, the spectral efficiency only increases 1 bit/s/Hz. In summary, through reasonable matching of splitting ratio and input power, the system's data transmission spectrum efficiency can reach up to 20 bit/s/Hz, which proves that the system has the potential for high-rate communication.

E. Summary

In summary, after numerical evaluation and analysis, we can know that the proposed RB SWIPT scheme is capable of supporting 13 W electrical power for charging and 20 bit/s/Hz spectral efficiency for communication, with 13% energy conversion efficiency and 10 m transmission distance. Table II presents the performance comparison between our system and the state-of-art architectures. As can be seen, proposed RB SWIPT has advantages in providing high power, while simultaneously enabling high spectral efficiency and energy conversion efficiency.

IV. DISCUSSION

A. Self-alignment

Different from the narrow-beam orientation SWIPT technology, the RB system can achieve self-alignment due to its separating cavity structure and retro-reflectors. The separating cavity structure makes the system can spontaneously generate the resonant beam when an effective beam channel exists between the two reflectors and the gain medium. The retro-reflector has the ability to make the incident beam transmit back to the cavity along the original path after reflection.

In the proposed RB scheme, to inhibit the beam loss, the TIM is introduced. However, the self-alignment can still exist when the effective beam transmitting path is established. To prove the self-alignment performance, ray tracing simulation (open source software: <https://ricktu288.github.io/ray-optics/>) has been conducted. As presented in Fig. 15 (a), with the function of the TIM, the beam phase is changed, and the beam

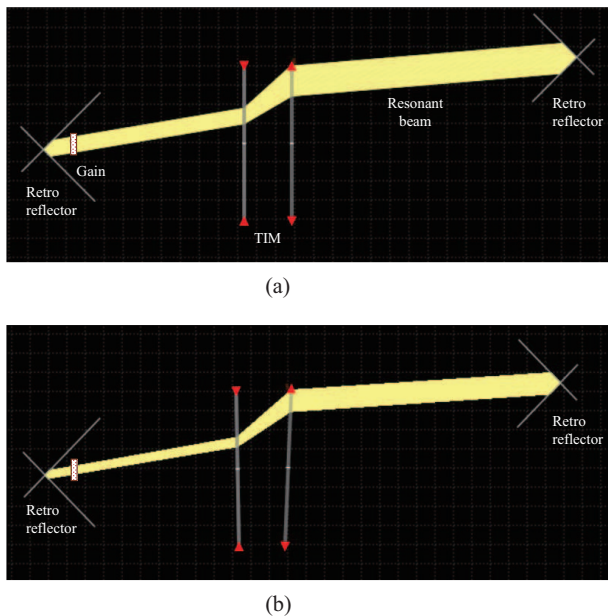


Fig. 15. Self-alignment simulation of the proposed system' cavity by ray tracing. (a) The beam direction is not perpendicular to the TIM surface, and the TIM's lenses are aligned; (b) The beam direction is not perpendicular to the TIM surface, and the TIM's lenses are not aligned.

spot is compressed. Moreover, the effective beam transmitting path can be achieved even if the direction is not perpendicular to the TIM surface. The situation of the TIM's lenses being not aligned is also tested. As shown in Fig. 15(b), both the concave lens and convex lens are tilted, while the rays in the cavity can still be captured. A little misalignment of the TIM does not break the capability of the self producing of the resonant beam. However, the tilt angle should be as small as possible to ensure TIM's function of beam compression ability. Therefore, lenses position holders, such as lens tubes, can be used in actual scenes.

B. Beam splitter

The carrier beam delivers both the energy and data from the transmitter to the receiver. However, due to the narrow bandwidth of PV, it faces the challenge to support high-frequency optical signal reception. Thus, we separate part of the external beam and use APD for signal reception. Beam splitters such as cube beam-splitters and plate beam-splitters can be used to separate the external beam. The structure of the beam splitters are demonstrated in Fig. 16. Cube beam-splitter (Fig. 16 a) consists of two classical right angle prisms which can be made by typical glasses such as N-BK7. The hypotenuse surface of one prism has a coating for beam splitting, and the two prisms are cemented together, forming a cubic shape. When the incident beam pass through the cube, it will be separate into the reflected beam and the emergent beam, accompanying by the energy assigning under the split ratio μ . Plate beam-splitter (Fig. 16 b) makes by a glass plate that has been coated on the first surface of the substrate for beam splitting. Plate beam-splitter can be set for 45-degree,

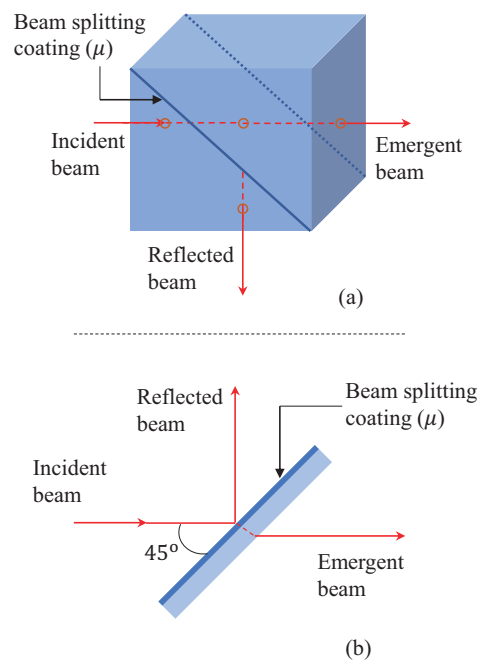


Fig. 16. Beam splitters diagram, (a) cube beam-splitter; (b) plate beam-splitter

when beams incident, part of the beam will transmit through it, and the other part of the beam is reflected by the coating and propagates in the vertical incident direction.

Challenges that the beam splitter may face. i) Generally, the reflection coefficient of the coating in a commercial splitter is an integer with errors, such as 20 ± 1 , 40 ± 2 , etc. According to the simulation calculation, if the reflection coefficient accurate to single digits is required, a high-performance, low-error reflection coating needs to be customized. ii) When the beam passes through the beam splitter, energy loss will occur due to the reflection. Therefore, each beam incident surface needs to be coated with an anti-reflection coating. iii) The impact that the beam incident with non-perpendicular (Cube beam-splitters) or 45-degree (Plate beam-splitters) into beam splitters needs to be considered.

V. CONCLUSIONS

In this paper, we proposed a high-efficiency resonant beam charging and communication system using the semiconductor gain medium and the telescope internal modulator. Relying on theories of beam transmission, energy harvesting, and data receiving, we have established analytical models for the beam transmission, energy output, and spectral efficiency of the proposed system. The numerical results illustrate that the system present a remarkable SWIPT performance. Compared with the original system with the solid-state gain medium without the telescope internal modulator, the energy conversion efficiency is increased by 13 times.

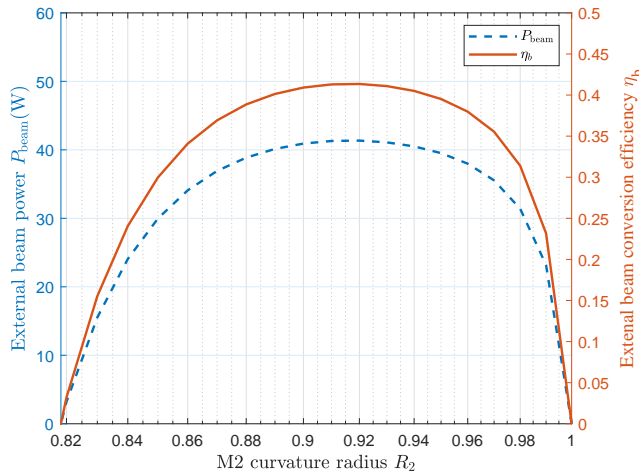


Fig. 17. M2's reflectivity versus external beam power and beam conversion efficiency ($P_{in} = 100W$)

APPENDIX A

THE IMPACT OF THE M2'S REFLECTIVITY ON OUTPUT BEAM POWER AND CONVERSION EFFICIENCY

From Fig. 11 and 12, we find that the performance of the beam power and conversion efficiency will be influenced by M2's reflectivity. Fig. 17 presents the curves of R_2 versus P_{beam} and η_b . It can be seen from the blue dotted line that, as the value of R_2 increases from 0.8 to 1, the power will first increase and then decrease, and the maximum value is 40 W when $R_2 \approx 0.92$. The solid red line shows the relationship between η_b and R_2 . The trend of the curve is the same as the power change curve. When R_2 takes nearly 0.92, the conversion efficiency can reach 0.43. From the curves, we can obtain the influence law of R_2 on P_{beam} and η_b , and obtain the optimal value of R_2 that satisfies the extreme performance of the system. It is worth noting that when R_2 is less than 0.8, there is no power output, which indicates that the loss of the system is greater than the gain at this time, and the beam channel cannot be established.

REFERENCES

- [1] M. Series, "IMT vision—framework and overall objectives of the future development of IMT for 2020 and beyond," *Recommendation ITU*, vol. 2083, 2015.
- [2] K. Jin and W. Zhou, "Wireless laser power transmission: a review of recent progress," *IEEE transactions on power electronics*, vol. 34, no. 4, pp. 3842–3859, Jul. 2018.
- [3] S. Y. R. Hui, W. Zhong, and C. K. Lee, "A critical review of recent progress in mid-range wireless power transfer," *IEEE Transactions on Power Electronics*, vol. 29, no. 9, pp. 4500–4511, Mar. 2013.
- [4] X. Lu, P. Wang, D. Niyato, D. I. Kim, and Z. Han, "Wireless charging technologies: Fundamentals, standards, and network applications," *IEEE Communications Surveys & Tutorials*, vol. 18, no. 2, pp. 1413–1452, Nov. 2015.
- [5] J. Lim, T. S. Khwaja, and J. Ha, "Wireless optical power transfer system by spatial wavelength division and distributed laser cavity resonance," *Opt. Express*, vol. 27, no. 12, pp. A924–A935, Jun 2019.
- [6] Y. Huang and B. Clerckx, "Waveform design for wireless power transfer with limited feedback," *IEEE Transactions on Wireless Communications*, vol. 17, no. 1, pp. 415–429, Nov. 2017.
- [7] B. Scrosati and J. Garcke, "Lithium batteries: Status, prospects and future," *Journal of power sources*, vol. 195, no. 9, pp. 2419–2430, May. 2010.

- [8] N. Shinohara, *Wireless power transfer via radiowaves*. Wiley Online Library, 2014.
- [9] R. W. Habash, J. M. Elwood, D. Krewski, W. G. Lotz, J. P. McNamee, and F. S. Prato, "Recent advances in research on radiofrequency fields and health: 2004–2007," *Journal of Toxicology and Environmental Health, Part B*, vol. 12, no. 4, pp. 250–288, Aug. 2009.
- [10] H. Haken, "Laser theory," in *Light and Matter Ic/Licht und Materie Ic*. Springer, 1970, pp. 1–304.
- [11] Q. Zhang, W. Fang, Q. Liu, J. Wu, P. Xia, and L. Yang, "Distributed laser charging: A wireless power transfer approach," *IEEE Internet of Things Journal*, vol. 5, no. 5, pp. 3853–3864, Oct. 2018.
- [12] W. Wang, Q. Zhang, H. Lin, M. Liu, X. Liang, and Q. Liu, "Wireless energy transmission channel modeling in resonant beam charging for IoT devices," *IEEE Internet of Things Journal*, vol. 6, no. 2, pp. 3976–3986, Apr. 2019.
- [13] M. Liu, H. Deng, Q. Liu, J. Zhou, M. Xiong, L. Yang, and G. B. Giannakis, "Simultaneous mobile information and power transfer by resonant beam," *IEEE Transactions on Signal Processing*, pp. 1–1, May. 2021.
- [14] M. A. Khalighi and M. Uysal, "Survey on free space optical communication: A communication theory perspective," *IEEE communications surveys & tutorials*, vol. 16, no. 4, pp. 2231–2258, Jun. 2014.
- [15] H. Li and Y. Huang, "The architecture of blind equalizer for mimo free space optical communication system," in *Optical Communication, Optical Fiber Sensors, and Optical Memories for Big Data Storage*, vol. 10158. International Society for Optics and Photonics, Oct. 2016, p. 101581H.
- [16] W. Fang, H. Deng, Q. Liu, M. Liu, Q. Jiang, L. Yang, and G. B. Giannakis, "Safety analysis of long-range and high-power wireless power transfer using resonant beam," *IEEE Transactions on Signal Processing*, May. 2021.
- [17] W. Chen, S. Zhao, Q. Shi, and R. Zhang, "Resonant beam charging-powered UAV-assisted sensing data collection," *IEEE Transactions on Vehicular Technology*, vol. 69, no. 1, pp. 1086–1090, Oct. 2019.
- [18] X. Liu, Y. Liu, Y. Chen, and L. Hanzo, "Trajectory design and power control for multi-UAV assisted wireless networks: A machine learning approach," *IEEE Transactions on Vehicular Technology*, vol. 68, no. 8, pp. 7957–7969, May. 2019.
- [19] M. Xiong, M. Liu, Q. Zhang, Q. Liu, J. Wu, and P. Xia, "TDMA in adaptive resonant beam charging for IoT devices," *IEEE Internet of Things Journal*, vol. 6, no. 1, pp. 867–877, Feb. 2018.
- [20] M. Xiong, Q. Liu, M. Liu, X. Wang, and H. Deng, "Resonant beam communications with photovoltaic receiver for optical data and power transfer," *IEEE Transactions on Communications*, vol. 68, no. 5, pp. 3033–3041, Feb. 2020.
- [21] M. S. Aziz, S. Ahmad, I. Husnain, A. Hassan, and U. Saleem, "Simulation and experimental investigation of the characteristics of a pv-harvester under different conditions," in *2014 International Conference on Energy Systems and Policies (ICESP)*. IEEE, Nov. 2014, pp. 1–8.
- [22] J. C. Campbell, "Recent advances in telecommunications avalanche photodiodes," *Journal of Lightwave Technology*, vol. 25, no. 1, pp. 109–121, Jan 2007.
- [23] M. Born and E. Wolf, *Principles of optics: electromagnetic theory of propagation, interference and diffraction of light*. Elsevier, 2013.
- [24] P. Baues, "Huygens' principle in inhomogeneous, isotropic media and a general integral equation applicable to optical resonators," *Opto-electronics*, vol. 1, no. 1, pp. 37–44, Feb. 1969.
- [25] H. Kogelnik, "Imaging of optical modes-resonators with internal lenses," *Bell System Technical Journal*, vol. 44, no. 3, pp. 455–494, Mar. 1965.
- [26] V. Magni, "Multielement stable resonators containing a variable lens," *JOSA A*, vol. 4, no. 10, pp. 1962–1969, Oct 1987.
- [27] M. Eichhorn, *Laser physics: from principles to practical work in the lab*. Springer Science & Business Media, 2014.
- [28] R. N. N. Hodgson and I. H. Weber, *Laser Resonators and Beam Propagation*. Springer, 2005, vol. 108.
- [29] W. Koehler, *Solid-state laser engineering*. Springer, 2013, vol. 1.
- [30] W. W. Chow, S. W. Koch, and M. I. Sargent, *Semiconductor-laser physics*. Springer Science & Business Media, 2012.
- [31] H. Soda, K. ichi Iga, C. Kitahara, and Y. Suematsu, "GaInAsP/InP surface emitting injection lasers," *Japanese Journal of Applied Physics*, vol. 18, no. 12, pp. 2329–2330, dec 1979.
- [32] H. Soda, Y. Motegi, and K. Iga, "GaInAsP/InP surface emitting injection lasers with short cavity length," *IEEE Journal of Quantum Electronics*, vol. 19, no. 6, pp. 1035–1041, Jun. 1983.
- [33] M. Kuznetsov, F. Hakimi, R. Sprague, and A. Mooradian, "Design and characteristics of high-power (0.5-W CW) diode-pumped

- vertical-external-cavity surface-emitting semiconductor lasers with circular TEM₀₀ beams," *IEEE Journal of Selected Topics in Quantum Electronics*, vol. 5, no. 3, pp. 561–573, May. 1999.
- [34] Q. Zhang, W. Fang, M. Xiong, Q. Liu, J. Wu, and P. Xia, "Adaptive resonant beam charging for intelligent wireless power transfer," *IEEE Internet of Things Journal*, vol. 6, no. 1, pp. 1160–1172, Feb. 2018.
- [35] E. Boshkovska, D. W. K. Ng, N. Zlatanov, and R. Schober, "Practical non-linear energy harvesting model and resource allocation for swipt systems," *IEEE Communications Letters*, vol. 19, no. 12, pp. 2082–2085, Dec. 2015.
- [36] F. Xu, M. Khalighi, and S. Bourennane, "Impact of different noise sources on the performance of PIN- and APD-based FSO receivers," in *Proceedings of the 11th International Conference on Telecommunications*, Jun. 2011, pp. 211–218.
- [37] A. Lapidot, S. M. Moser, and M. A. Wigger, "On the capacity of free-space optical intensity channels," *IEEE Transactions on Information Theory*, vol. 55, no. 10, pp. 4449–4461, Oct. 2009.
- [38] M. S. Demir, F. Miramirkhani, and M. Uysal, "Handover in VLC networks with coordinated multipoint transmission," in *2017 IEEE International Black Sea Conference on Communications and Networking (BlackSeaCom)*, Jun. 2017, pp. 1–5.
- [39] C. Quintana, Q. Wang, D. Jakonis, X. Piao, G. Erry, D. Platt, Y. Thueux, A. Gomez, G. Faulkner, H. Chun, M. Salter, and D. O'Brien, "High speed electro-absorption modulator for long range retroreflective free space optics," *IEEE Photonics Technology Letters*, vol. 29, no. 9, pp. 707–710, Mar. 2017.
- [40] A. J. Moreira, R. T. Valadas, and A. de Oliveira Duarte, "Optical interference produced by artificial light," *Wireless Networks*, vol. 3, no. 2, pp. 131–140, May. 1997.
- [41] S. Ma, F. Zhang, H. Li, F. Zhou, Y. Wang, and S. Li, "Simultaneous lightwave information and power transfer in visible light communication systems," *IEEE Transactions on Wireless Communications*, vol. 18, no. 12, pp. 5818–5830, Dec. 2019.
- [42] A. M. Abdelhady, O. Amin, B. Shihada, and M.-S. Alouini, "Spectral efficiency and energy harvesting in multi-cell swipt systems," *IEEE Transactions on Wireless Communications*, vol. 19, no. 5, pp. 3304–3318, Feb. 2020.
- [43] I. Krikidis, S. Timotheou, S. Nikolaou, G. Zheng, D. W. K. Ng, and R. Schober, "Simultaneous wireless information and power transfer in modern communication systems," *IEEE Communications Magazine*, vol. 52, no. 11, pp. 104–110, Nov. 2014.
- [44] X. Lu, P. Wang, D. Niyato, and E. Hossain, "Dynamic spectrum access in cognitive radio networks with rf energy harvesting," *IEEE Wireless Communications*, vol. 21, no. 3, pp. 102–110, Jun. 2014.